Conductance fluctuations induced by bulk state in quasi-one-dimensional strips of topological insulator

Y. Takagaki[*]

Paul-Drude-Institut für Festkörperelektronik, Hausvogteiplatz 5-7, 10117 Berlin, Germany
(Received 10 February 2012; revised manuscript received 20 March 2012; published 9 April 2012)

We numerically calculate the conductance of a topological insulator confined as quasi-one-dimensional strips using a four-band Hamiltonian. The conductance is nearly unchanged in the presence of a short-range disorder when the Fermi level is located in the bulk band gap. Helical edge states of topological insulators are no longer protected against the disorder, and scattering takes place if the bulk state coexists. Both the magnitude of conductance fluctuations and the average conductance are found to vary nonmonotonically in the latter regime with the strength of disorder, where the fluctuation amplitude is reduced when the *average* conductance is around $2e^2/h$. The scattering of the topological states is hence evidenced to be nontrivially affected by the coupling with the bulk state.

I. INTRODUCTION

The bulk band gap of topological insulators (TIs) contains gapless metallic surface states having a linear dispersion. These states are helical, i.e., the orientation of spin is locked to be perpendicular to the direction of propagation.[1,2] As nonmagnetic impurities do not flip the spin in reversing the momentum of an electron by scattering, time reversal symmetry forbids backscattering for the helical TI states.[3,4] The absence of scattering gives rise to quantum spin Hall effect, where a spin current flows without dissipation.[5] The quantum spin Hall effect has the potential to allow us to manipulate the electron spin purely electrically without using ferromagnetic materials or an external magnetic field. The helical states in TIs are thus attractive for spintronics.

Anderson localization for Dirac fermions and its consequences on the quantum spin Hall effect were investigated theoretically.[6–9] For topological protection from scattering, the energy gap arising from the spin-orbit interaction plays a crucial role. Although the quantum spin Hall effect produced by the robust topological order was predicted initially for graphene,[10] the spin-orbit interaction in graphene was soon recognized to be too weak for the topological protection to be relevant. Nonetheless, the absence of backscattering has been experimentally demonstrated alternatively for the edge states in HgTe quantum wells,[11] which are two-dimensional (2D) TIs, and for the surface states in $Bi_{1-x}Sb_x$[12] and Bi_2Te_3,[13] which are three-dimensional (3D) TIs.

The robustness against external perturbations in TIs breaks down in some circumstances. In this paper, we investigate a breakdown caused by the coexistence of the bulk state.[14] Although we treat a 2D TI as a model system, our findings may be relevant to the reproducible magnetoconductance fluctuations observed in Bi_2Se_3 samples.[15] In the 3D TIs Bi_2Se_3, Bi_2Te_3, and Sb_2Te_3, crystal vacancies provide free carriers and thus the Fermi level is typically located outside the bulk band gap. These materials are narrow-band-gap semiconductors, and so the influence of the bulk state is hard to avoid even if the Fermi level is brought into the band gap by a carrier compensation.

We present the results of numerical simulations on the conductance of quasi-one-dimensional (quasi-1D) strips of a TI in which a short-range disorder is imposed. We examine the variations of the average conductance and the amplitude of conductance fluctuations when the disorder is strengthened. We show that not only the fluctuation amplitude but also the average conductance can change nontrivially with the disorder strength. A correlation between the fluctuation amplitude and the average conductance is identified, which is pronounced when the Fermi level is located just above the threshold of the bulk 1D sub-bands.

II. NUMERICAL MODEL

To describe the electronic states in 2D TIs, we used the effective four-band Hamiltonian,[2,16,17]

$$H = \begin{pmatrix} C_k + M_k & Ak_+ & -iRk_- & -\Delta \\ Ak_- & C_k - M_k & \Delta & 0 \\ iRk_+ & \Delta & C_k + M_k & -Ak_- \\ -\Delta & 0 & -Ak_+ & C_k - M_k \end{pmatrix}, \quad (1)$$

defined on a basis $(|e+\rangle,|h+\rangle,|e-\rangle,|h-\rangle)$, where e and h denote, respectively, the electron and hole bands and $\pm$ refers to the spin orientation. Here, $C_k = -D(k_x^2 + k_y^2)$, $M_k = M - B(k_x^2 + k_y^2)$, and $k_\pm = k_x \pm ik_y$. Two types of spin-orbit coupling (Δ and the electron Rashba term controlled by the parameter R) due to the breaking of bulk inversion symmetry were taken into account.[2,17] The material parameters were chosen to be appropriate for HgTe quantum wells,[2,17] as listed in Table I.

We considered narrow strips prepared from a 2D TI having a uniform width of 100 nm. The conductance G of the strips was determined using the Landauer formula $G = (e^2/h)\text{Tr}[t^\dagger t]$, where the transmission matrix t was calculated using the lattice Green's function method.[18] The strips were approximated by a square lattice having a lattice parameter a (see the Appendix).[17–19] A short-range disorder[17,20,21] was introduced by modifying the on-site energy randomly by amounts distributed uniformly within an interval $[-U/2,U/2]$. The length

TABLE I. Parameters for the effective four-band Hamiltonian corresponding to HgTe quantum wells.[2,17]

M	-0.01 eV
D	-0.5 nm^2 eV
B	-0.7 nm^2 eV
A	0.365 nm eV
R	-0.016 nm eV
Δ	0.0016 eV

of the disorder region was set to be 2 μm. Unless stated otherwise, i.e., except in Fig. 4, we assumed $a = 2$ nm and the statistical properties of the conductance were evaluated using, at least, 500 disorder realizations. For the critical features in the conductance fluctuations that we describe below, the statistical reliability was checked by increasing the number of disorder ensembles up to 1000.

III. RESULTS AND DISCUSSION

In Fig. 1, we show the dispersion of 1D sub-bands in the 100-nm-wide strip. The negative value of M implies that the energy edge of the electron band is lower than that of the hole band. The overlapped electron and hole bands generate a Dirac cone when a coupling between the bands is turned on through the terms in H associated with the parameter A. The Dirac point, which is indicated by the arrow in Fig. 1, opens a gap when the 2D system is confined laterally as a quasi-1D strip. For energies higher than 22.0 meV for the conduction band and lower than -15.2 meV for the valence band, bulk 1D sub-bands are also occupied at the Fermi level. As one finds, the spin degeneracy is lifted in our simulations due to the spin-orbit coupling.
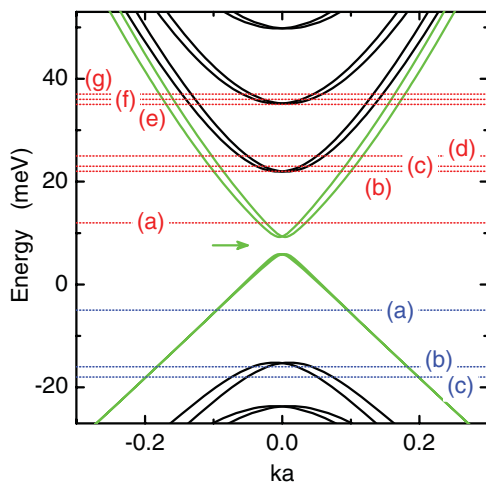

FIG. 1. (Color online) Energy band structure in a quasi-one-dimensional strip of a topological insulator. Parameters were chosen to correspond to a 100-nm-wide strip produced from a HgTe quantum well. The wave number k was calculated using a tight-binding model with a lattice constant $a = 2$ nm. The arrow indicates the Dirac point when lateral confinement is absent. Conductance characteristics plotted in Figs. 2 and 3 were calculated for the Fermi energies represented by the dotted lines.
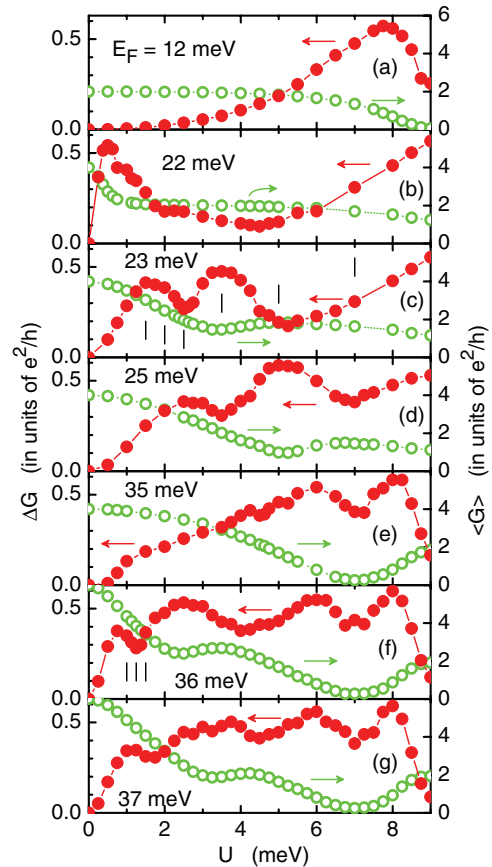

FIG. 2. (Color online) Dependence of the amplitude of conductance fluctuations ΔG (filled circles) and the average conductance $\langle G \rangle$ (open circles) on the strength U of short-range disorder. The Fermi energy E_F was chosen to be 12, 22, 23, 25, 35, 36, and 37 meV, from top to bottom. The width of the topological insulator strip is 100 nm. The length of the disordered region is 2 μm. The lattice constant a of the square lattice used for the simulations was set to be 2 nm. The statistical uncertainties are smaller than the symbols. Bars in (c) and (f) indicate the disorder strengths assumed in Fig. 5.

The evolution of the average conductance $\langle G \rangle$ and the amplitude of conductance fluctuations $\Delta G = \langle (G - \langle G \rangle)^2 \rangle^{1/2}$ when the disorder is strengthened is shown in Figs. 2 and 3 for n- and p-type conductions, respectively. Here, $\langle \cdots \rangle$ denotes averaging over disorder realizations. The Fermi energy E_F was set to the values indicated by the dotted lines in Fig. 1.[22] As shown in Figs. 2(a) and 3(a), the conductance is nearly unaffected by the disorder when the bulk state is unoccupied,[20,21] i.e., $\langle G \rangle \approx 2e^2/h$ and $\Delta G \approx 0$. The topological protection for the helical edge states from backscattering breaks down in this circumstance only if the disorder is strong [see Fig. 2(a)].

When the Fermi level exceeds the threshold for the lowest bulk 1D sub-band in the conduction band [Figs. 2(b)–2(g)], the conductance fluctuations emerge as soon as the disorder is imposed. The amplitude of the universal conductance fluctuations (UCFs) in ordinary conductors is $0.73e^2/h$ and $0.365e^2/h$ in the absence and presence of spin-orbit interaction, respectively.[23–25] While ΔG changes nonmonotonically with U, the peak values of ΔG are comparable with these universal amplitudes. In particular, in Fig. 3(c), where the first
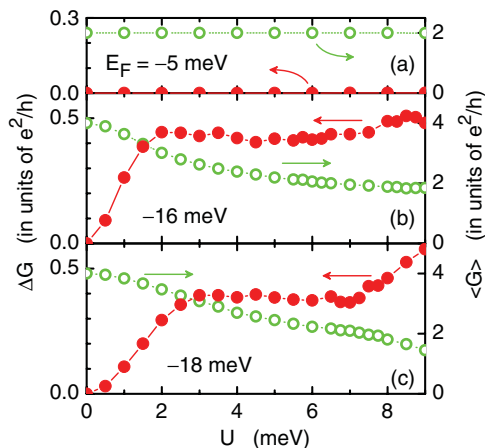
FIG. 3. (Color online) Dependence of the amplitude of conductance fluctuations ΔG (filled circles) and the average conductance $\langle G \rangle$ (open circles) on the strength U of short-range disorder when the Fermi level is located in the valence band. The Fermi energy E_F is (a) -5 meV, (b) -16 meV, and (c) -18 meV. The lattice constant a of the square tight-binding lattice was set to be 2 nm. The statistical uncertainties are smaller than the symbols.

bulk 1D sub-band in the valence band is occupied, ΔG is nearly identical to the value for the case of strong spin-orbit interaction.

The initial decay in $\langle G \rangle$ as U is increased becomes slower in Figs. 2(b)−2(e) for higher Fermi energies. The increase in the kinetic energy for the bulk 1D sub-band is plausibly responsible for this suppression of the scattering. When the Fermi level is just above the threshold of the bulk sub-band [Fig. 2(b)], $\langle G \rangle$ develops a plateau for moderate values of U (=2–6 meV). The plateau value $2e^2/h$ suggests that the TI states are almost completely transmitted owing to the topological protection, whereas the bulk state is almost fully localized by the disorder because of its negligibly low kinetic energy. The conductance fluctuations peaked at $U \approx 0.5$ meV are thus attributed to the bulk sub-band. The characteristics for $U > 5$ meV are similar to those shown in Fig. 2(a), and so they are indicated to be associated with the TI states. The small ΔG suggests that the localized bulk state in this situation provides almost no contribution to the conductance.

As E_F is increased to be away from the sub-band threshold, ΔG increases to be as large as expected for UCF over nearly the entire range of U. We emphasize that the high fluctuation amplitude implies that the conductance in this circumstance can be considerably lower than $2e^2/h$. That is, the TI states are no longer protected from scattering. Nevertheless, $\langle G \rangle$ remains at $\sim 2e^2/h$ in Fig. 2(c) over a wide range of U, giving rise to a plateau-like structure. The topological protection is thus suggested to be partly maintained when the Fermi level is not far from the sub-band threshold. Reflecting, presumably, this influence of the topological protection, we find a remarkable reduction in ΔG when the *average* conductance is approximately $2e^2/h$ at $U = 2.5$ and $5-5.5$ meV.

With increasing E_F, the plateau-like structure shifts to higher values of U and weakens. In the regime of the plateau-like structure, $\langle G \rangle$ does not decrease monotonically with increasing U. To illustrate these behaviors clearly,
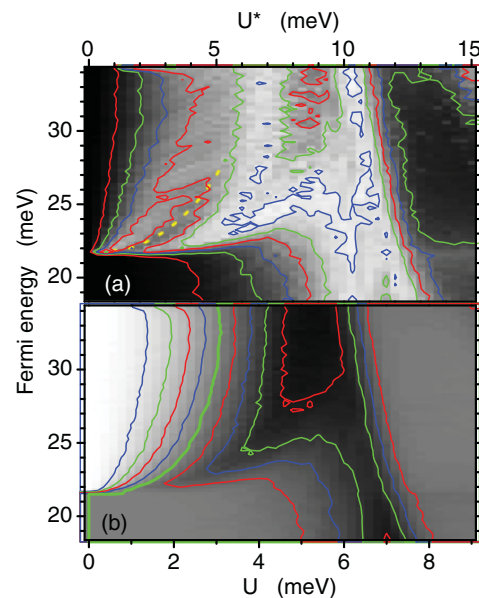

FIG. 4. (Color online) Gray-scale (and contour) plots of (a) fluctuation amplitude ΔG and (b) average conductance $\langle G \rangle$ when the Fermi energy and the strength U of disorder are varied. The maximum values and 0 are set to be, respectively, white and black for the gray scales. Statistical properties were calculated assuming the lattice parameter to be $a = 10/3$ nm and using 200 disorder realizations. The disorder strength U when $a = 10/3$ nm is equivalent to $U^* = \frac{5}{3}U$ when $a = 2$ nm. The dotted line in (a) indicates the dip when $\langle G \rangle$ crosses $2e^2/h$. The value of $\langle G \rangle$ for the thick line in (b) is $2e^2/h$.

we plot $\langle G \rangle$ and ΔG in Fig. 4 using gray scales. Here, we assumed $a = 10/3$ nm and used 200 disorder ensembles for evaluating the conductance statistics in order to lighten the computational load. The mean free path associated with the short-range disorder is proportional to $(Ua)^{-2}$, and so the disorder strength for $a = 10/3$ nm is equivalent to $U^* = \frac{5}{3}U$ when $a = 2$ nm.

As shown in Fig. 4(a), a valley develops between the quantized conductance at $U = 0$ and the plateau-like structure for large U. Both the valley and the plateau-like regions shift to larger U with increasing E_F. One finds in Fig. 4(b) that ΔG is enhanced in the domain of the valley in $\langle G \rangle$. The suppression in ΔG when $\langle G \rangle$ crosses $2e^2/h$, which is indicated by the thick solid line in Fig. 4(b), in the course of transition between the quantized conductance at $U = 0$ and the conductance valley is unambiguously visible. As highlighted by the dotted curve in Fig. 4(a), the dip appears to emerge at $U = 0$ when the Fermi level crosses the sub-band threshold. The behaviors of $\langle G \rangle$ and ΔG are even more puzzling when $U > 6$ meV.

In order to gain insight into the peculiar characteristics of ΔG and $\langle G \rangle$, we compare in Fig. 5(a) the distributions of the conductance when $E_F = 23$ meV for various values of U. There we plot the probability $P(g)$ for the conductance to be lower than g. In the metallic limit, a Gaussian distribution of conductance is expected for UCF.[26] For $U = 1.5$ meV, the spread of the Gaussian conductance distribution is above $2e^2/h$. We anticipate that the conductance fluctuations in this case arise solely from the bulk state, while the TI states are unaffected by the disorder. This explains the near-UCF
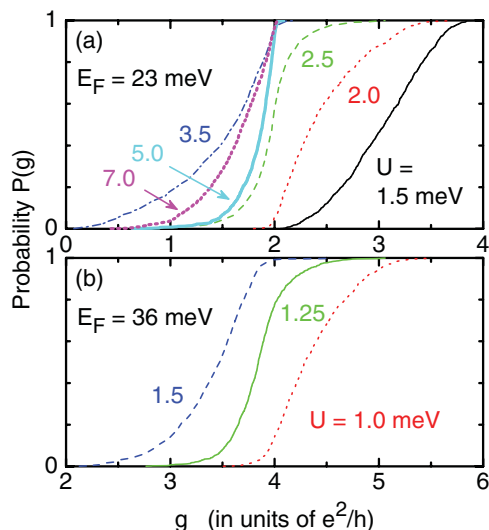
FIG. 5. (Color online) Probability $P(g)$ for the conductance to be lower than g when the Fermi energy E_F is (a) 23 meV and (b) 36 meV. The magnitude U of the disorder is 1.5, 2.0, 2.5, 3.5, 5.0, and 7.0 meV, respectively, for the thin solid, thin dotted, dashed, dash-dotted, thick solid, and thick dotted curves in (a) and 1.0, 1.25, and 1.5 meV, respectively, for the dotted, solid, and dashed curves in (b).

value for ΔG. The bulk state is roughly localized when U is 2.0−2.5 meV. The conductance is, as a consequence, distributed in a narrow range around the value of $2e^2/h$ provided by the TI states. As the bulk and TI states remain to be nearly decoupled,[27] the localized bulk state plays only a negligible role, and so ΔG decreases.

For $U > 2.5$ meV, the conductance values for most of disorder realizations become smaller than $2e^2/h$. The increase in ΔG to the level of the UCF value when $U = 3.5$ meV thus arises from the fact that the TI states are scattered here by the strong disorder. We point out that the distributions for $U = 2.0$ and 3.5 meV contain tails on the large- and small-G sides, respectively, in contrast to the nearly symmetric distribution for $U = 2.5$ meV. That is, the conductance distribution changes dramatically when ΔG develops a dip. The asymmetric shape of the distribution is hence considered to be a manifestation of the influence of the partly protected TI states.

Surprisingly, the topological protection for the TI states reappears when U is further increased to 5.0 meV. A forward-propagating electron in the helical edge state is likely scattered into the backward-propagating bulk sub-band when $U = 3.5$ meV. The bulk state will cease to act as the outgoing state when it is strongly localized by the disorder. In Fig. 5(a), the conductance when $U \geqslant 3.5$ meV is almost limited to be below $2e^2/h$, suggesting the almost-complete localization of the bulk state. The conductance fluctuations will then be suppressed, as the probability for a direct scattering between the helical edge states is still low. When $U = 7.0$ meV, the direct scattering probability is expected to increase significantly, similarly to the large-U case in Fig. 2(a), giving rise to an increase in ΔG and a decrease in $\langle G \rangle$.

The plateau-like structure in Fig. 2(e) takes place at large U as the Fermi level is far above the sub-band threshold. The suppression in ΔG when $\langle G \rangle \approx 2e^2/h$ persists, although it is fairly weak. These features reappear in the small-U

region when the Fermi level crosses the second bulk 1D sub-band [Figs. 2(f) and 2(g)]. The fluctuations are reduced when the average conductance exhibits a maximum at the end of the plateau-like structure, at $U \sim 4$ meV in Fig. 2(f) and $U \sim 4.5$ meV in Fig. 2(g). The anomalous features again shift to larger U and become smaller in magnitude with increasing E_F.

In comparison to the case associated with the threshold of the lowest bulk 1D sub-band, the plateau value is higher; i.e., the plateau is considerably above $2e^2/h$ in Fig. 2(f). Both the second-lowest and the lowest bulk 1D sub-bands are thus suggested to be involved in the transport when the plateau-like structure emerges. With respect to the reduction in ΔG that occurred in the course of transition from the quantized conductance at $U = 0$ to the conductance valley, the reduction is observed in Figs. 2(f) and 2(g) when $\langle G \rangle \approx 4e^2/h$. The distribution of conductance changes the shape markedly when U is varied around the value for the dip in ΔG. As shown in Fig. 5(b), the distribution for $U = 1.0$ and 1.5 meV again exhibits large- and small-G tails, respectively. We speculate that the localization of the second bulk sub-band is responsible for the reduction in ΔG, while the lowest bulk sub-band is almost fully transmitted, as the disorder is insignificant for the latter. In other words, the near-complete transmission for the TI and lowest bulk 1D states leads to $\langle G \rangle \approx 4e^2/h$.

In Figs. 2(e)−2(g), ΔG is also reduced when $U \sim 7$ meV. This reduction is, however, ascribed to the fact that the localization is strong, i.e., $\langle G \rangle < \Delta G$. In the strongly localized regime, $\ln G$ exhibits the Gaussian distribution rather than G.[28,29] It may be noteworthy that the statistical reliability of ΔG and $\langle G \rangle$ that we obtained by averaging G consequently deteriorates as they are dominated by the disorder realizations for which the conductance becomes high. This is plausibly responsible for the small irregular features in ΔG.

When the Fermi level is in the valence band, the topological protection is extremely robust against disorder, as shown in Fig. 3(a). The nonmonotonic features of ΔG and $\langle G \rangle$ are practically absent even when the Fermi level is just above the threshold of the bulk 1D sub-band [Fig. 3(b)]. The disorder-induced coupling with the bulk state is, therefore, indicated to cause merely the simple backscattering of the TI states for $U > 7$ meV. The increase in ΔG when $\langle G \rangle$ becomes smaller than $2e^2/h$ in Fig. 3(b) may be regarded as evidence that the bulk 1D hole sub-band generates conductance fluctuations corresponding to the case of strong spin-orbit interaction, whereas the spin-orbit interaction is effectively absent for the fluctuations produced by the TI states.

Throughout our simulations presented above, ΔG was smaller than $0.6e^2/h$. Although gigantic conductance fluctuations in a 3D TI were observed experimentally by Checkelsky *et al.*,[15] we find no enhancement of the fluctuation amplitude affected by the TI states in comparison to the value expected for ordinary conductors. We note, however, that the topological protection does not forbid scattering between the surface states in 3D TIs, as electrons do not have to be scattered in the backward direction, in contrast to 2D TIs. The conductance fluctuations in 2D and 3D TI systems may, therefore, exhibit different characteristics.

IV. CONCLUSIONS

In conclusion, we have numerically examined the quantum transport in 100-nm-wide quasi-1D strips constructed from a HgTe quantum well in the presence of a short-range disorder. The backscattering for the helical edge states in the TI is no longer absent when the bulk 1D sub-bands are occupied at the Fermi level, as scattering from the edge state to the bulk state is allowed. We have demonstrated that the amplitude of conductance fluctuations and the average conductance can change nonmonotonically when the disorder is strengthened. The unusual dependence on the disorder strength originates from the fact that the disorder-induced scattering between the TI and bulk states and the transition from the metallic transport regime to the localized transport regime for the bulk state take place at different scales of the disorder strength. The anomalous features are pronounced when the Fermi level is just above the sub-band threshold, as the barely occupied sub-band is strongly localized by disorder.

APPENDIX: TIGHT-BINDING MODEL

The effective four-band Hamiltonian, Eq. (1), is mapped onto a 2D square tight-binding lattice as

$$H_{\text{TB}} = \sum_{i,j} V_{ij} c_{ij}^{\dagger} c_{ij} + \sum_{i,j} (T_x c_{i+1,j}^{\dagger} c_{ij} + T_y c_{i,j+1}^{\dagger} c_{ij} + \text{H.c.}),$$
(A1)

where $c_{ij}^{\dagger}$ and c_{ij} are the creation and annihilation operators at the lattice site (i,j), respectively. The on-site elements V_{ij} are given by

$$V_{ij} = \begin{pmatrix} M_+ - E_F & 0 & 0 & -\Delta \\ 0 & M_- - E_F & \Delta & 0 \\ 0 & \Delta & M_+ - E_F & 0 \\ -\Delta & 0 & 0 & M_- - E_F \end{pmatrix},$$
(A2)

where $M_{\pm} = \pm M - 4(D \pm B)$ and E_F is the Fermi energy. The nearest-neighbor hopping elements V_x and V_y are given for the longitudinal direction as

$$V_x = \begin{pmatrix} D+B & iA/2 & R/2 & 0 \\ iA/2 & D-B & 0 & 0 \\ -R/2 & 0 & D+B & -iA/2 \\ 0 & 0 & -iA/2 & D-B \end{pmatrix}$$
(A3)

and for the transverse direction as

$$V_y = \begin{pmatrix} D+B & -A/2 & -iR/2 & 0 \\ A/2 & D-B & 0 & 0 \\ -iR/2 & 0 & D+B & -A/2 \\ 0 & 0 & A/2 & D-B \end{pmatrix}.$$
(A4)

The wave function is set to vanish outside the lattice, and so the width W of a strip consisting of N transverse lattice sites, for instance, is given as $W = (N+1)a$.

*takagaki@pdi-berlin.de

[1]B. A. Bernevig, T. L. Hughes, and S.-C. Zhang, Science **314**, 1757 (2006).

[2]M. König, H. Buhmann, L. W. Molenkamp, T. L. Hughes, C.-X. Liu, X.-L. Qi, and S.-C. Zhang, J. Phys. Soc. Jpn. **77**, 031007 (2008).

[3]C. Wu, B. A. Bernevig, and S.-C. Zhang, Phys. Rev. Lett. **96**, 106401 (2006).

[4]C. Xu and J. E. Moore, Phys. Rev. B **73**, 045322 (2006).

[5]C. L. Kane and E. J. Mele, Phys. Rev. Lett. **95**, 146802 (2005).

[6]P. M. Ostrovsky, I. V. Gornyi, and A. D. Mirlin, Phys. Rev. Lett. **98**, 256801 (2007).

[7]S. Ryu, C. Mudry, H. Obuse, and A. Furusaki, Phys. Rev. Lett. **99**, 116601 (2007).

[8]J. H. Bardarson, J. Tworzydło, P. W. Brouwer, and C. W. J. Beenakker, Phys. Rev. Lett. **99**, 106801 (2007).

[9]K. Nomura, M. Koshino, and S. Ryu, Phys. Rev. Lett. **99**, 146806 (2007).

[10]C. L. Kane and E. J. Mele, Phys. Rev. Lett. **95**, 226801 (2005).

[11]M. König, S. Wiedmann, C. Brüne, A. Roth, H. Buhmann, L. Molenkamp, X.-L. Qi, and S.-C. Zhang, Science **318**, 766 (2007).

[12]P. Roushan, J. Seo, C. V. Parker, Y. S. Hor, D. Hsieh, D. Qian, A. Richardella, M. Z. Hasan, R. J. Cava, and A. Yazdani, Nature (London) **460**, 1106 (2009).

[13]T. Zhang, P. Cheng, X. Chen, J.-F. Jia, X. Ma, K. He, L. Wang, H. Zhang, X. Dai, Z. Fang, X. Xie, and Q.-K. Xue, Phys. Rev. Lett. **103**, 266803 (2009).

[14]S. Kim, M. Ye, K. Kuroda, Y. Yamada, E. E. Krasovskii, E. V. Chulkov, K. Miyamoto, M. Nakatake, T. Okuda, Y. Ueda, K. Shimada, H. Namatame, M. Taniguchi, and A. Kimura, Phys. Rev. Lett. **107**, 056803 (2011).

[15]J. G. Checkelsky, Y. S. Hor, M.-H. Liu, D.-X. Qu, R. J. Cava, and N. P. Ong, Phys. Rev. Lett. **103**, 246601 (2009).

[16]A. Roth, C. Brüne, H. Buhmann, L. W. Molenkamp, J. Maciejko, X.-L. Qi, and S.-C. Zhang, Science **325**, 294 (2009).

[17]D. G. Rothe, R. W. Reinthaler, C.-X. Liu, L. W. Molenkamp, S.-C. Zhang, and E. M. Hankiewicz, New J. Phys. **12**, 065012 (2010).

[18]T. Ando, Phys. Rev. B **44**, 8017 (1991).

[19]Y. Takagaki and Y. Tokura, Phys. Rev. B **54**, 6587 (1996).

[20]L. Sheng, D. N. Sheng, C. S. Ting, and F. D. M. Haldane, Phys. Rev. Lett. **95**, 136602 (2005).

[21]M. Onoda, Y. Avishai, and N. Nagaosa, Phys. Rev. Lett. **98**, 076802 (2007).

[22]As the ratio between the strip sizes and the Fermi wavelength provides generally the scaling behavior of the numerical results, changing the Fermi energy is, in principle, equivalent to changing the width and length of the strips.

[23]P. A. Lee, A. D. Stone, and H. Fukuyama, Phys. Rev. B **35**, 1039 (1987).

[24]These values are for a quasi-1D system. For 2D and quantum dot systems, the fluctuation amplitude in the absence of spin-orbit interaction is $0.86e^2/h$ and $0.70e^2/h$, respectively. The amplitude is, in any case, reduced by half by the spin-orbit interaction.

[25] Tight-binding simulations of UCFs in ordinary conductors in the presence of spin-orbit coupling have been presented by, for instance, T. Kaneko, M. Koshino, and T. Ando, Phys. Rev. B **81**, 155310 (2010).

[26] M. C. W. van Rossum, I. V. Lerner, B. L. Altshuler, and T. M. Nieuwenhuizen, Phys. Rev. B **55**, 4710 (1997).

[27] Y. Okada, C. Dhital, W. Zhou, E. D. Huemiller, H. Lin, S. Basak, A. Bansil, Y.-B. Huang, H. Ding, Z. Wang, S. D. Wilson, and V. Madhavan, Phys. Rev. Lett. **106**, 206805 (2011).

[28] A. Douglas and K. A. Muttalib, Phys. Rev. B **80**, 161102(R) (2009).

[29] Y. Takagaki and D. K. Ferry, J. Phys. Condens. Matter **4**, 10421 (1992).